Journal of Materials Science & Technology 276 (2027) 31–35

Contents lists available at ScienceDirect

Journal of Materials Science & Technology

journal homepage: www.elsevier.com/locate/jmst

Letter

Is the strain hardening rate minimal for a GPa-yield-strength alloy with a yield ratio close to unity?

Yuanyue Zhao [a], Yan Ma [b], Jungwan Lee [b], Chang Liu [a,*], En (Evan) Ma [a,*]

[a] Center for Alloy Innovation and Design (CAID), State Key Lab for Mechanical Behavior of Materials, Xi'an Jiaotong University, Xi'an 710049, China
[b] Department of Materials Science and Engineering, Delft University of Technology, Delft NL-2628 CD, Netherlands

ARTICLE INFO

Article history:
Received 12 March 2026
Revised 23 March 2026
Accepted 24 March 2026
Available online 16 April 2026

Keywords:
Multi-principal-element alloy
Bcc
Yield ratio
Strain hardening

ABSTRACT

The engineering stress-strain curve is often observed to be flat across a wide range of plastic strains after yielding in a uniaxial tensile test, for alloys with gigapascal yield strength, especially those recently developed body-centered-cubic (bcc) multi-principal-element alloys (MPEAs). The near-zero slope of these curves is often perceived as an apparent lack of strain hardening capability, which would set off necking immediately after yielding due to a violation of the Considère criterion. If so, how could the alloy manage to sustain the large uniform elongation? Here, we resolve this puzzle by re-analyzing the data in terms of true stress versus true strain to demonstrate that the perception above is a misjudgment. Thanks to the MPEA's gigapascal yield strength, the wide plateau does not mean that the strain hardening rate is negligible, but rather is at GPa level, adequate to guarantee no onset of the necking instability. Inside a tensile-strained TiZrNb MPEA, the dislocation density was observed to increase by nearly two orders of magnitude, even after a tensile strain of only 8%, indicating obvious dislocation accumulation as the mechanism for strain hardening to delay necking. All these corroborate that an alloy yielding at GPa stress with a "perfect-plastic" curve is ultra-strong yet highly ductile, despite its very high (i.e., almost ∼1) yield ratio.

Many alloys developed during the past two decades, especially GPa-yield-strength ones, including recent body-centered-cubic (bcc) multi-principal-element alloys (MPEAs), have shown a tensile engineering stress-strain curve that looks almost "perfectly plastic". Even though the yield point phenomenon is absent, right after yielding, the curve plateaus across a wide range of plastic strains [1–5], leading to a minimal strain hardening coefficient (n). Three previously published high-impact examples of such curves are given in Fig. 1. The earliest case of the three is a Fe-Mn-Ni-Ti-Mo-C maraging steel [6] in Fig. 1(a). This ultrahigh-strength steel shows almost constant GPa flow stress across ∼12% tensile elongation. The second example displayed in Fig. 1(b) is a bcc $HfNbTiVAl_{10}$ alloy [1], which shows a yield strength (σ_y) of 1390 MPa and an ultimate tensile strength (σ_{UTS}) of 1416 MPa. Here, the yield ratio, defined as the ratio of the σ_y to the σ_{UTS}, is 1390/1416=0.98. Such a value close to unity is on the extreme side of high-yield-ratio alloys, which normally have a yield ratio larger than ∼0.8 [7]. The curve is nearly flat for the regime of ∼20% uniform elongation. As yet another representative, the $Ti_{36}V_{14}Nb_{22}Hf_{22}Zr_1Al_5$ (at.%) alloy from our own lab also exhibits a wide stress plateau from the yielding point to a strain of 25%, and its yield ratio is as high as 0.99, Fig. 1(c) [5]. A high yield-ratio is not desirable for demanding applications, because the alloy would be subject to plastic instabilities upon overloading or during forming operations, and exhibit inadequate energy absorption [8–10].

Looking at these engineering stress-strain curves, one is tempted to jump to the following conclusion. First, because the slope of the stress-strain curve in the plastic regime is nearly zero, the alloy's strain hardening rate is believed to be lower than, by far, metals having a much lower strength but a rising stress-strain curve after yielding. The above expectation is in line with the common wisdom that a high yield ratio close to unity is synonymous with little or no strain hardening capability. Such a weak strain hardening ability would then be expected to translate into a high propensity for plastic instability [11], as predicted by the Considère criterion. That is, for such high-σ_y alloys, the strain hardening rate cannot keep up with the high flow stress, such that the alloy would be expected to succumb to necking immediately after yielding in a uniaxial tensile test. The uniform elongation achievable would therefore be very small. From this standpoint, the quite large uniform tensile ductility, i.e., the uniform strain surpassing 20% elongation before the stress falls off in the stress-strain curves

* Corresponding authors.
E-mail addresses: maen@xjtu.edu.cn (E. Ma), chang.liu@xjtu.edu.cn (C. Liu).

https://doi.org/10.1016/j.jmst.2026.03.071
1005-0302/

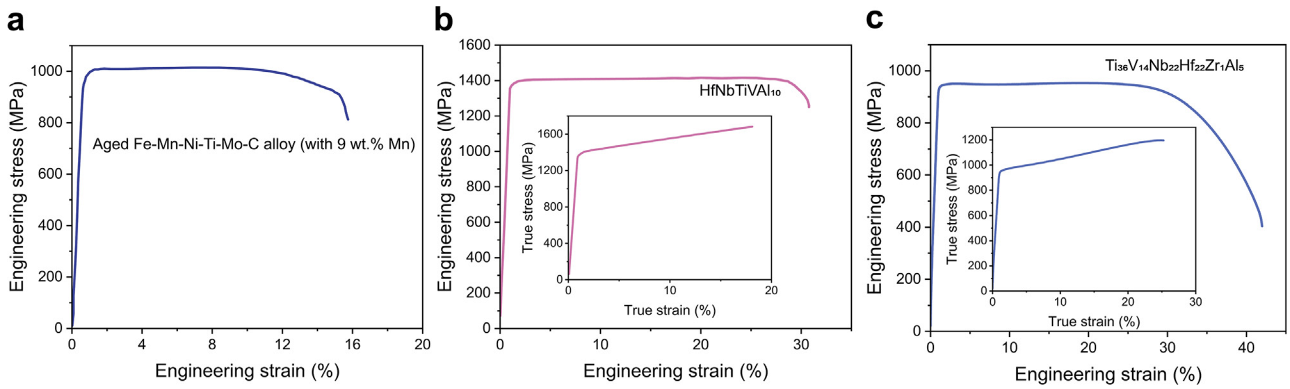

Fig. 1. The engineering tensile stress-strain curve of (a) A Fe-Mn-Ni-Ti-Mo-C maraging steel, adapted from Ref. [6], (b) A bcc $HfNbTiVAl_{10}$ alloy, adapted from Ref. [1]; The inset is the corresponding true stress-strain curve, and (c) A $Ti_{36}V_{14}Nb_{22}Hf_{22}Zr_1Al_5$ (at.%) alloy made and tested in our lab, adapted from [5]. The inset displays the corresponding true stress-strain curve.

(Fig. 1), is not supposed to happen. This has become a puzzle begging for an answer, especially for students and new researchers in the field.

This Letter aims to clarify that the projection above arises from a misconception. We first demonstrate that when a high-yield-ratio alloy has a GPa-level σ_y, its true strain hardening rate (Θ) is actually also on that level, and the Θ can even be higher than alloys with a relatively low σ_y and lower yield ratio. Secondly, such an alloy is not destined to neck early; on the contrary, despite the barely positive slope of the engineering stress-strain curve, the available Θ is in fact adequate to maintain a fairly large uniform elongation in uniaxial tensile deformation under GPa flow stresses.

Strain hardening. Fig. 2 displays a schematic for a hypothetical engineering stress-strain curve (solid curve in red) in a tensile test. This simplified curve represents high-σ_y alloys similar to those in Fig. 1, each of which shows a stress-strain behavior that could be approximated by a straight line, with a high yield ratio close to unity at room temperature. The red curve in Fig. 2 gives a yield ratio of σ_y/σ_{UTS} =1000 MPa/1030 MPa=0.97. The benchmark to be compared is a more familiar (lower-σ_y) alloy, with a simplified curve (blue solid line). This reference alloy has a σ_y of 200 MPa and a σ_{UTS} of 300 MPa, and therefore a much lower yield ratio of (200/300=) 0.66. Its engineering stress-strain behavior in

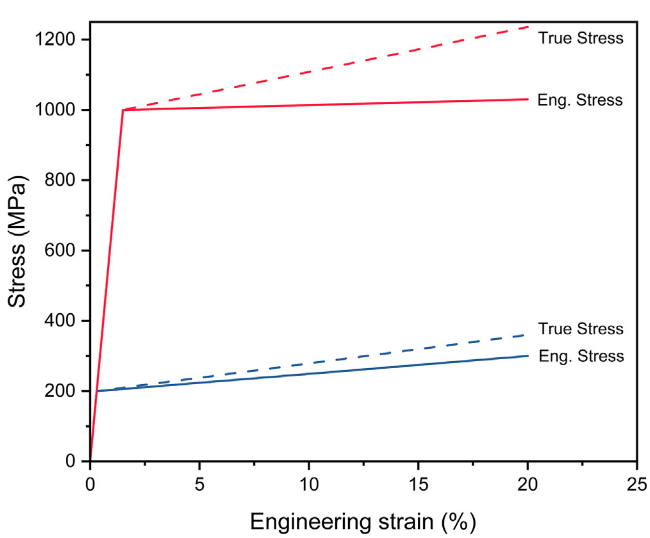

Fig. 2. A schematic diagram comparing different engineering stress-strain curves, which are hypothesized as straight lines (the linearity assumed for the true-stress curve approximates those in Fig. 1, but is a rather crude simplification by assuming a constant stress and small engineering strains, see equations below) to allow quick analysis and explanation.

Fig. 2 shows a curve going upward with an obvious slope (solid blue curve).

Looking at the curves, one may think the blue material/curve with a lower yield ratio (0.66) strain hardens more than the flatter red one. However, after converting the curves into true stress-true strain (dashed lines), it turns out the upper alloy with a high yield ratio (0.97) gains more strength from strain hardening: at ε_e = 20%, for example, the difference between the dashed and solid red curves is obviously larger than that between the blue ones.

Let us do some simple math to quantify which curve has strain-hardened more, after 20% strain beyond yielding. We begin with the red curve in Fig. 2, which shows a σ_y of 1000 MPa, and the flow stress at 20% strain is 1030 MPa. The strain-hardening gain at this point is merely 30 MPa, corresponding to an engineering (subscript e) strain hardening rate of $d\sigma_e/d\varepsilon_e$ = 30/0.2 = 150 MPa, as the curve is so flat (similar to the experimental high-strength bcc curves seen in Fig. 1). However, similar to the case in the inset of Fig. 1(b, c)), one should note that the corresponding gain in true stress is much more pronounced, as seen from the true stress curve (dashed red) in Fig. 2.

One could also do the engineering-to-true conversion by making use of the standard Eqs. (1) and (2) below [12], assuming uniform cross-sectional area across the gauge length, because the engineering curve does not bend over (i.e., peaking and then falling), indicating no necking throughout the tensile test.

$$\sigma_T = \sigma_e(1+\varepsilon_e) \tag{1}$$

$$\varepsilon_T = \ln(1+\varepsilon_e) \tag{2}$$

$$\begin{aligned}\frac{d\sigma_T}{d\varepsilon_T} &= \frac{d\sigma_e + \varepsilon_e d\sigma_e + \sigma_e d\varepsilon_e}{d\varepsilon_e/(1+\varepsilon_e)} \\ &= (1+\varepsilon_e)\left[\frac{d\sigma_e}{d\varepsilon_e} + \varepsilon_e\frac{d\sigma_e}{d\varepsilon_e} + \sigma_e\right] \\ &= (1+\varepsilon_e)\left[\frac{d\sigma_e}{d\varepsilon_e}(1+\varepsilon_e) + \sigma_e\right] \\ &= \left[(1+\varepsilon_e)^2\frac{d\sigma_e}{d\varepsilon_e} + \sigma_e(1+\varepsilon_e)\right]\end{aligned} \tag{3}$$

For small ε_e,

$$\cong \frac{d\sigma_e}{d\varepsilon_e} + \sigma_e \tag{4}$$

To put the true (subscript T) strain hardening rate, $\Theta = d\sigma_T/d\varepsilon_T$, in semi-quantitative terms, Eq. (4) can be used in conjunction with the schematic Fig. 2 to give a crude approximation. The estimated Θ is 1180 MPa, which is not a low rate at all, and is actually higher than the Θ ~800 MPa of the lower blue curve/alloy (this is to be contrasted with the engineering curves mentioned earlier: the blue alloy yields at 200 MPa, rising to 300 MPa at ε_e ~20%, such that its $d\sigma_e/d\varepsilon_e = 500$ MPa, much higher than the 150 MPa of the red curve). Such a Θ comparison can also be carried out via a more rigorous calculation using Eq. (3) directly, in lieu of the hypothetical Fig. 2 or the simplified Eq. (4). In any case, nevertheless, the alloy corresponding to the red curve turns out to strain-hardens at a faster Θ, by as much as ~50%, than the alloy showing the blue curve, even though from the engineering curves one is led to think the opposite.

In general, one should always use caution when interpreting an engineering curve, which assumes a constant cross-sectional area and is thus a misrepresentation of the real stress experienced by the sample. An extreme case is after necking, when the engineering curve descends continuously, suggesting that a decreasing stress would be able to keep pulling the sample to larger and larger strains. This is obviously not true, as the true stress inside the necked region actually keeps going up all the time. By the same token, strain hardening before necking should also be gauged using the true stress-strain derivative, $d\sigma_T/d\varepsilon_T$, rather than the $d\sigma_e/d\varepsilon_e$.

From Eqs. (3) and (4) above, we envision different scenarios for the true strain hardening rate ($\Theta = d\sigma_T/d\varepsilon_T$) of the alloys undergoing uniform elongation. (i) We see that $d\sigma_T/d\varepsilon_T$ is always higher than what is observed from the slope in the engineering curve ($d\sigma_e/d\varepsilon_e$), which controls only the first term on the right-hand side of Eqs. (3) or (4); $d\sigma_e/d\varepsilon_e$ is only part of the real strain hardening, at best only the effect of the latter bestowed on the nominal (engineering) stress-strain curve. To gauge the true $d\sigma_T/d\varepsilon_T$, there is a second term that needs to be added, which clearly shows the role of the stress level (σ_e). (ii) We can use the simplified Eq. (4) containing only two terms to roughly assess their relative weight of contribution, which is different for the high-strength and low-strength alloys. For the low-σ_y alloys, the second σ_e term is not so significant and the $d\sigma_e/d\varepsilon_e$ term is what we take to gauge strain hardening; we are accustomed to doing so on regular basis, and would take $d\sigma_e/d\varepsilon_e$ => 0 to imply diminishing $d\sigma_T/d\varepsilon_T$. But, for high-σ_y alloys, in Eq. (4) the σ_e term outweighs the $d\sigma_e/d\varepsilon_e$ term and is in fact predominant. When $d\sigma_e/d\varepsilon_e = 0$, that only shows the applied load reaches its maximum in the tensile test, while there is still ongoing strain hardening ($d\sigma_T/d\varepsilon_T$). (iii) Therefore, we conclude that when it comes to comparing the Θ of the two alloys in Fig. 2, the one with much higher σ_y wins. This can be further appreciated by examining some extreme cases. Imagine a case when both the red solid curve and the blue solid curve have the same slope ($d\sigma_e/d\varepsilon_e$). Then, it is the second term in Eq. (4) that determines which alloy gives higher $d\sigma_T/d\varepsilon_T$. That is, the red curve starting at a much higher σ_y is favored. In another limiting case, when $d\sigma_e/d\varepsilon_e$ approaches zero for both alloys, $d\sigma_T/d\varepsilon_T$ scales directly with σ_e. Again, the red curve wins over the blue one.

As such, the common expectation that a near-flat engineering stress-strain curve equals little strain hardening should not be taken for granted. In particular, the perception that high-σ_y MPEAs have no strain-hardening capability is incorrect. It is also not necessarily true that an apparently flat engineering stress-strain curve indicates a lower Θ relative to a steeper curve; the opposite can happen. To determine which curve strain-hardens more requires a comparison of the true stress-strain curves, to account for the level of actual flow stress experienced in the tensile sample.

The continuous storage of forest and geometrically necessary dislocations into the alloy is a common cause of strain hardening during tensile straining. This is also the case for alloys in Fig. 1. As demonstrated before in Ref. [5], the sample in Fig. 1(c) was characterized using a transmission electron microscope (TEM), which revealed a continuously rising density of dislocations after plastic strains of 5%, 10%, and 20%. In Fig. 3, we show a more global characterization of dislocation density in a single-phase bcc TiZrNb MPEA, which again exhibits a flat engineering stress-strain curve (Fig. 3(a)) similar to those cited in Fig. 1 [1,5,6]. The TiZrNb alloy was prepared via arc melting high-purity Ti, Zr, and Nb (with purities exceeding 99.95 wt%) in a Ti-gettered high-purity argon atmosphere, remelted five times to achieve chemical homogeneity, and then cast into a 50 g ingot. The as-cast alloy was then cold-rolled with a 75% thickness reduction (from 4 to 1 mm). The resulting sheet was subsequently annealed at 900 °C for 5 min, followed by water quenching to room temperature. We used this example to directly measure the density of dislocations accumulated inside. Through synchrotron X-ray diffraction analysis of the diffraction peak line profiles, the dislocation density was calculated using the modified Williamson-Hall (MWH) method [13–15]. The results demonstrate that tensile straining raised the dislocation density by two orders of magnitude, from 0.05×10^{14} m^{-2} before test to 2.4×10^{14} m^{-2} after only 8% strain, which is an elongation much lower than those in Fig. 1. The contribution of dislocation accumulation to the flow stress elevation at this strain is 52 MPa, quantified by applying the Taylor hardening model that gives $\Delta\sigma_{\text{dislocation}} = M\alpha Gb\sqrt{\rho}$ [16], where M is the Taylor factor ($M = 2.733$ in bcc alloys [17]), α the Taylor constant, G the shear modulus, b the magnitude of the Burgers vector, and ρ the dislocation density. This magnitude is close to that (~60 MPa) measured in the tensile test (see true-stress vs true-strain curve in Fig. 3(a)). This result clearly shows that dislocation accumulation remains a potent work-hardening mechanism. A 60 MPa increase would be deemed effective strain hardening in a low-σ_y alloy with σ_y =100 MPa, as the engineering stress would have gained by half of σ_y after only 8% of strain, clearly showing a rising curve with an obvious slope of $d\sigma_e/d\varepsilon_e$~500 MPa. But for the case of σ_y~870 MPa in Fig. 3(a), the true stress gain of ~60 MPa would correspond to little change in terms of engineering stress on the plateau. The presence of a sizable Θ becomes obvious only from the true stress vs true strain curve (the inset in Fig. 3(a)).

Resistance to necking. Observing the curves in Fig. 1, necking would seem imminent right after yielding, when considering that for a GPa-σ_y alloy, to resist necking its $d\sigma_T/d\varepsilon_T$ would have to start at the GPa level to keep up with the high σ_T [5], as mandated by the Considère criterion,

$$\Theta = \frac{d\sigma_T}{d\varepsilon_T} > \sigma_T \tag{5}$$

From our discussion above, it should be recognized that the true Θ in Fig. 1 is, in fact, on such a high level, rather than close to zero. To hammer home our point that uniform elongation can indeed be sustained, let us revisit the simplified curves/analysis in Fig. 2. Here, the red engineering curve is much flatter relative to the blue one, but its Θ is actually larger, because its low $\frac{d\sigma_e}{d\varepsilon_e}$ term is compensated by the high second term (see Eq. (4) above). Let us look at Eq. (3) again to see what it would predict. Even though the $\frac{d\sigma_e}{d\varepsilon_e}$ is barely positive, $\frac{d\sigma_T}{d\varepsilon_T}$ would nevertheless remain larger than $\sigma_e(1+\varepsilon_e)$, i.e., Θ stays above σ_T, ensuring that $\frac{d\sigma_T}{d\varepsilon_T} > \sigma_T$ is upheld. As such, the Considère criterion for maintaining stable tensile plastic flow would not be violated. To see the above from equations, the critical condition to avoid necking from the governing Considère criterion in Eq. (5) can be translated into one for the engineering stress-strain curve, using the connections shown in Eq. (3),

$$\frac{d\sigma_T}{d\varepsilon_T} = (1+\varepsilon_e)\left[\frac{d\sigma_e}{d\varepsilon_e}(1+\varepsilon_e)+\sigma_e\right] > \sigma_T \tag{6}$$

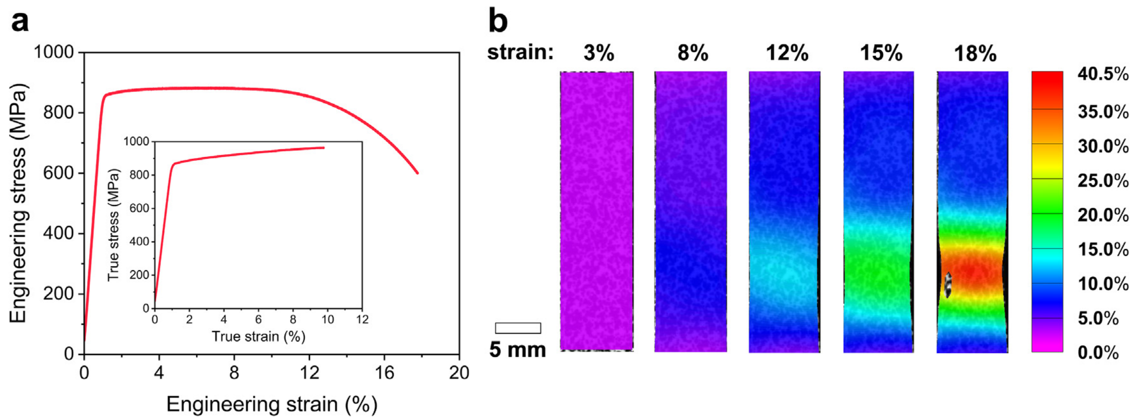

Fig. 3. A bcc TiZrNb MPEA, as another example of high-yield-ratio bcc alloys. (a) Tensile engineering stress-strain curve of the TiZrNb alloy. The inset is the corresponding true stress-true strain curve. (b) Strain distribution across the gauge length in the TiZrNb alloy upon uniaxial pulling, as measured in situ using digital-image-correlation (DIC) during the tensile test. The color bar represents different levels of engineering strain.

Substituting σ_T with Eq. (1) leads to

$$\frac{d\sigma_e}{d\varepsilon_e}(1+\varepsilon_e)+\sigma_e > \sigma_e \tag{7}$$

i.e.,

$$\frac{d\sigma_e}{d\varepsilon_e} > 0 \tag{8}$$

which explicitly gives the relevant condition preceding the onset of necking, normally recognized to correspond to the maximum point in the engineering curve, where $d\sigma_e/d\varepsilon_e = 0$ (and $d\sigma_e/d\varepsilon_e < 0$ afterwards as the σ_e falls down with necking). In other words, as long as a positive slope (no matter how small) is sustained during tensile straining, the near-flat engineering curves in Fig. 1 (or the red curve in Fig. 2) offer adequate $d\sigma_T/d\varepsilon_T$ to ward off plastic flow instability. This explains the seemingly anomalous plateau of uniform strain (prolonged to > 20% uniform elongation) observed in Fig. 1. Putting it another way, the fact that the engineering curve (in Fig. 1) sustains a very shallow yet positive slope ($d\sigma_e/d\varepsilon_e > 0$), by itself alone, signals that the $d\sigma_T/d\varepsilon_T$ of the alloy is sufficiently high to delay necking. As a result, an appreciable uniform strain can be achieved, even though the alloy has a GPa-level σ_y with a yield ratio so close to unity.

The absence of necking across strains across the flat portion of the stress-strain curve is confirmed for our TiZrNb example in Fig. 3. In this sample, we monitored the plastic strain distribution along the gauge length during tension using digital image correlation (DIC). As shown in Fig. 3(b), the first ~8% plastic strain appears to be mostly uniform (i.e., it stays on a single-digit level across the board, see the strain magnitude bar in Fig. 3(b)). The strain localization becomes obvious only after ~8% strain, followed by clear necking. This result corroborates that necking does not take off, as the flat curve still presents a decent level of strain hardening *via* dislocation accumulation.

We mention in passing that, generally speaking, there can be additional mechanisms that enhance dislocation accumulation and strain hardening to sustain a flat engineering stress-strain curve. For instance, nanoprecipitates that help trap dislocations (Fig. 1(a) [6]), phase transformations with transformation-induced plasticity (TRIP) effects [18], and local chemical orders that boost geometrically necessary dislocations and back stresses [19] have all been discussed in the literature. The latter two examples [18,19] under very high stresses, in fact, pose demanding requirements for significant strain hardening in the Lüders band, in order to force the Lüders front [20] to propagate outward across the gauge length to extend the yield plateau [21]. While this discontinuous yielding does not change the general applicability of the conclusions above, a treatment of the dynamics sustaining the wide yield plateau in the presence of highly localized yet stably propagating Lüders strains needs to be elaborated elsewhere in the future.

Summary remarks. Our take-home message is the following. One should not accept *a priori* the popular expectation that an apparently flat engineering stress-strain curve means little or no strain hardening. This projection does not hold for a high-σ_y material. It is also not true that a flat engineering stress-strain curve always indicates a lower strain hardening rate relative to a higher-slope curve. We have shown that a high-σ_y alloy exhibiting a flat engineering stress-strain curve actually implies a rather high true strain hardening rate Θ (i.e., $d\sigma_T/d\varepsilon_T$), which can be even higher than an alloy with an engineering curve showing a larger slope but yields at a much lower σ_y. As derived from Eq. (3), a GPa-σ_y bcc alloy with a yield ratio as high as ~1 can carry a GPa-level strain hardening rate and a fairly large uniform tensile elongation, as observed in Fig. 1. Such alloys' strain-hardening capability (adequate Θ) that delays the necking instability, thanks to the observed capability to store dislocation, has previously been under-appreciated.

The above conclusions are applicable to all alloys, as the deduction does not invoke specifics in the microstructure, such as crystal structure, local chemical order, dislocation slip modes, etc. For GPa-σ_y bcc alloys, one would particularly strive for a steeply rising engineering stress-strain curve to impart even more pronounced strain hardening than what has been achieved in the examples discussed in this Letter. The challenge lies in finding additional strain hardening capability to enhance and supplement the dislocation accumulation (as measured above, along with tensile straining). By contrast, many face-centered-cubic alloys, including recently developed MPEAs, readily reach high Θ, because in those cases twinning-induced plasticity (TWIP)/ TRIP mechanisms or nanoprecipitates [22–24] are more hardening-effective. On the bcc side, such mechanisms have been less invoked. As a result, a bcc alloy having concurrently a σ_y at GPa-level, a relatively low-yield-ratio, and an extensive uniform tensile elongation till an ultrahigh σ_{UTS}, remains to be developed.

Declaration of competing interest

The authors declare that they have no known competing financial interests or personal relationships that could have appeared to influence the work reported in this paper.

CRediT authorship contribution statement

Yuanyue Zhao: Visualization, Validation, Investigation, Formal analysis, Data curation. **Yan Ma:** Resources, Data curation. **Jungwan Lee:** Resources, Data curation. **Chang Liu:** Writing – review & editing, Supervision, Resources. **En (Evan) Ma:** Writing – review & editing, Writing – original draft, Supervision, Conceptualization.

Acknowledgment

This work was financially supported by the National Natural Science Foundation of China (No. 52231001).

References

[1] Z.B. An, A. Li, S.C. Mao, T. Yang, L.Y. Zhu, R. Wang, Z.X. Wu, B. Zhang, R.W. Shao, C. Jiang, B.X. Cao, C.J. Shi, Y. Ren, C. Liu, H.B. Long, J.F. Zhang, W. Li, F. He, L.G. Sun, J.B. Zhao, L.Y. Yang, X.Y. Zhou, X. Wei, Y.M. Chen, Z.G. Lu, F.Z. Ren, C.T. Liu, Z. Zhang, X.D. Han, Nature 625 (2024) 697–702.
[2] S.L. Wei, S.J. Kim, J.Y. Kang, Y. Zhang, Y.J. Zhang, T. Furuhara, E.S. Park, C.C. Tasan, Nat. Mater. 19 (2020) 1175–1181.
[3] Y. Su, Y. Chen, Z. Lu, S. Wang, Z. Wang, X. Gao, L. Wang, X. Zeng, Scr. Mater. 267 (2025) 116825.
[4] L. Wang, J. Ding, S.S. Chen, K. Jin, Q.H. Zhang, J.X. Cui, B.P. Wang, B. Chen, T.Y. Li, Y. Ren, S.J. Zheng, K.S. Ming, W.J. Lu, J.H. Hou, G. Sha, J. Liang, L. Wang, Y.F. Xue, E. Ma, Nat. Mater. 22 (2023) 950–957.
[5] Z. Wang, X. Chen, D. Zhang, G. Wu, Y. Ma, X. Zeng, Z. Rao, C. Liu, E. Ma, Proc. Natl. Acad. Sci. 123 (2026) e2530922123.
[6] D. Raabe, D. Ponge, O. Dmitrieva, B. Sander, Scr. Mater. 60 (2009) 1141–1144.
[7] EN 1993-1-8:2005 - Design of steel structures - Part 1-8: Design of joints, 2005.
[8] J.H. Gross, J. Eng. Ind. 93 (1971) 962–968.
[9] H. Yamanouchi, B. Kato, H. Aoki, Mater. Struct. 23 (1990) 305–315.
[10] Q.M. Yang, H.Y. Ban, Thin-Walled Struct. 184 (2023) 110470.
[11] E. Ma, T. Zhu, Mater. Today 20 (2017) 323–331.
[12] W.D. Pilkey, Formulas For stress, strain, and Structural matrices, 2nd, Hoboken, NJ, John Wiley & Sons, 2005.
[13] T. Ungár, J. Gubicza, G. Ribárik, A. Borbély, J. Appl. Cryst. 34 (2001) 298–310.
[14] T.W. Lu, B.H. Sun, Y. Li, S. Dai, N. Yao, W.B. Li, X.Z. Dong, X.Y. Chen, J.C. Niu, F. Ye, A.K. da Silva, S.Y. Zhu, Y. Xie, X.F. Yang, S.H. Deng, J.P. Tan, Z.M. Li, D. Ponge, L.H. He, X.C. Zhang, D. Raabe, S.T. Tu, Nature 645 (2025) 385–391.
[15] L. Liu, Q. Yu, Z. Wang, J. Ell, M.X. Huang, R.O. Ritchie, Science 368 (2020) 1347–1352.
[16] M. Delincé, Y. Bréchet, J.D. Embury, M.G.D. Geers, P.J. Jacques, T. Pardoen, Acta Mater. 55 (2007) 2337–2350.
[17] J.M. Rosenberg, H.R. Piehler, Metall. Trans. 2 (1971) 257–259.
[18] B.B. He, B. Hu, H.W. Yen, G.J. Cheng, Z.K. Wang, H.W. Luo, M.X. Huang, Science 357 (2017) 1029–1032.
[19] B.W. Xu, H.C. Duan, X.F. Chen, J. Wang, Y. Ma, P. Jiang, F.P. Yuan, Y.D. Wang, Y. Ren, K. Du, Y.G. Wei, X.L. Wu, Nat. Mater. 23 (2024) 755–761.
[20] N. Maruyama, M. Yamamoto, S. Tabata, ISIJ Int. 63 (2023) 899–909.
[21] S. Yan, Z.F. Yu, T.S. Liang, S. Wang, W.D. Li, X. Tao, X.H. Liu, Mater. Des. 235 (2023) 112380.
[22] Z.M. Li, K.G. Pradeep, Y. Deng, D. Raabe, C.C. Tasan, Nature 534 (2016) 227–230.
[23] T. Yang, Y.L. Zhao, W.P. Li, C.Y. Yu, J.H. Luan, D.Y. Lin, L. Fan, Z.B. Jiao, W.H. Liu, X.J. Liu, J.J. Kai, J.C. Huang, C.T. Liu, Science 369 (2020) 427–432.
[24] E. Ma, C. Liu, Prog. Mater. Sci. 143 (2024) 101252.